Detection of structures in the horizontal wind field over complex terrain using coplanar Doppler lidar scans

Bianca Adler[1,2,3*], Norbert Kalthoff[1] and Olga Kiseleva[1]

[1]Institute of Meteorology and Climate Research, Karlsruhe Institute of Technology, Karlsruhe, Germany
[2]Current affiliation: CIRES, University of Colorado, Boulder, CO, USA
[3]Current affiliation: NOAA Physical Sciences Laboratory, Boulder, CO, USA

Abstract

Coplanar scans from three Doppler lidars are used to retrieve the horizontal wind field in a horizontal plane of about $5\,\text{km} \times 5\,\text{km}$ in size above the city of Stuttgart in south-western Germany. Stuttgart is located in moderate mountainous terrain that is characterized by a basin-shaped valley (Stuttgart basin) which opens into the larger Neckar Valley. Using the retrieved horizontal wind field, which is available on 22 days with a temporal resolution of 1 min and a horizontal resolution of 100 m, we investigate the mesoscale structure of the horizontal flow in the valleys with respect to time of the day, stratification and wind above the mean ridge height, and determine how fast the cells in the convective boundary layer move downstream, i.e. we estimate the convection velocity. The measurements reveal a large spatial and temporal variability of the flow. During stable conditions, the flow below the mean ridge height is decoupled from the flow aloft and downvalley wind dominates in the valleys. At the opening of the Stuttgart basin into the Neckar Valley outflow dominates during nighttime, whereas inflow into the basin prevails in the early morning. During thermally unstable conditions the flow in the valleys is mainly coupled to the flow aloft with a preference for upvalley wind direction. Convective cells moving downstream are detected in the horizontal wind field and a method to estimate the convection velocity from the horizontal wind field measurements is presented. The mean convection velocity is found to be higher by 24 % than the mean horizontal wind speed at the same height and about similar to the wind speed 100 m further up.

Keywords: urban atmospheric boundary layer, convection velocity, mountainous terrain, thermally driven circulation, convective cells, Urban Climate Under Change [UC][2]

1 Introduction

The atmospheric boundary layer (ABL) over complex terrain is highly variable in space and time. This is due to the superposition and interaction of processes on multiple scales. Convection, shear-driven turbulence and mesoscale thermally driven circulations (e.g. Adler and Kalthoff, 2014; Serafin et al., 2018) as well as dynamically driven flows which form when air flows over orography (e.g. Jackson et al., 2013; Adler and Kalthoff, 2016) interact with each other and impact the conditions in the ABL. The flow structure in the ABL is crucial for the exchange of air masses in valleys and basins with the layers aloft, i.e. for the ventilation. In particular in inhabited valleys and basins, the air quality strongly depends on this ventilation (e.g. Steyn et al., 2013). Examples of populated valleys, which have been probed in meteorological field campaigns, are the Lower Fraser Valley (e.g. Steyn et al., 1997) and the Salt Lake City Valley (e.g. Allwine et al., 2002; Lareau et al., 2013) in the USA, the Inn Valley in Austria (e.g. Gohm et al., 2009; Haid et al., 2020) and the Rhine Valley in south-western Germany (e.g.

Kalthoff and Vogel, 1992; Kalthoff et al., 1998; Kossmann et al., 1998). The large spatial variability of the flow induced by the orography and the built-up areas imposes high demands on the observation strategy as observation with a high spatial and temporal resolution are necessary to capture the variability and characteristics of the flow (e.g. Barlow, 2014). Point measurements on towers are not only of limited representativeness, they are also difficult to install in built-up areas and capture only the lowest part of the ABL.

To investigate the spatial characteristics of the convective ABL, such as the size of the turbulent cells, the standard set-up involves in situ measurements on towers. This means that the temporal measurements have to be transferred to corresponding spatial measurements. Under the assumption that the timescale of the cells is longer than the time it takes the cell to be advected past the point where the measurement is taken, Taylor's hypothesis can be used to transfer temporal measurements to space using the so called convection velocity (Townsend, 1976, Chapter 1.7), i.e. the velocity with which the cells propagate downstream. As the convection velocity is usually not directly measured, a mean horizontal wind speed is often used for the transfer. This assumption is critical for various reasons, i.e. the cells do not necessarily move with the mean wind speed at the

*Corresponding author: Bianca Adler, NOAA/ESRL/PSL, R/PSD3, 325 Broadway, Boulder, CO 80305-3328, USA, e-mail: bianca.adler@noaa.gov

probed height, not all cells travel with the same velocity depending on their spatial dimensions, and the convection velocity may not be constant with time (e.g. POWELL and ELDERKIN, 1974; DEL ÁLAMO and JIMÉNEZ, 2009). Using an array of tower measurements, HAN et al. (2019) studied the influence of the convection velocity on the applicability of Taylor's hypothesis in estimating the streamwise length scale of structures in the surface layer. They found that the global convection velocity is approximately 16 % larger than the mean streamwise velocity component at the same height and that the values of the streamwise length scale obtained from Taylor's hypothesis agrees better with the values of the streamwise length scale obtained from spatially-separated measurements when the convection velocity is used instead of the mean streamwise velocity component. The uncertainty arising from slight changes of the convection velocity can even explain some of the differences in turbulence parameters in the convective ABL calculated from temporal Doppler lidar measurements and spatial aircraft measurements (ADLER et al., 2019). Unless an array of multiple 100-m towers can be installed, tower measurements can only be used to deduce the convection velocity in the surface layer. This is not only very expensive, but may even be impossible over complex topography such as cities or mountainous terrain. In order to get information on the convection velocity of cells in the middle and upper part of the ABL or over highly complex terrain, another type of measurement is thus necessary to provide simultaneous measurements at several locations in space with a high temporal resolution allowing the convective cells to be resolved.

Combining measurements from several Doppler lidars is a promising approach to investigate both of the above described topics, i.e. the mesoscale variability of the flow over complex terrain and the displacement of cells in the convective ABL, as they can provide simultaneous wind measurements at many locations (separated by several tens of meters) in a large area (few square kilometers) which are not accessible by traditional in situ measurements, e.g. above buildings. As a Doppler lidar can only measure the radial velocity along the line-of-sight, the combination of two or more lidars is one possible approach to get information on the wind vector. One possible configuration is to perform coplanar vertical range height indicator (RHI) scans with several lidars and to retrieve the two-dimensional wind field in the overlapping area (e.g. NEWSOM et al., 2008). This approach provides the two-dimensional wind vector in a vertical plane and was e.g. used to study intrusions and waves in a Meteor crater basin in Arizona (WHITEMAN et al., 2018a; WHITEMAN et al., 2018b), to study wakes related to a wind energy turbine between two parallel mountain ridges (WILDMANN et al., 2018; MENKE et al., 2019; PALMA et al., 2019), or to analyze the cross-valley circulation in a major Alpine valley (ADLER et al., submitted). Another approach is to retrieve horizontal wind profiles with so-called virtual towers by performing simultaneous measurements of the same volume of air

from different azimuthal directions. This method was successfully applied over urban flat terrain (e.g. CALHOUN et al., 2006) and over urban mountainous terrain (WITTKAMP et al., submitted). A third possible configuration is to perform coplanar (near-)horizontal plan-position-indicator (PPI) scans with two or more Doppler lidars which allows the spatial distribution of the horizontal wind field to be retrieved. Already during the Joint Urban 2003 field campaign in Oklahoma City, Oklahoma, dual-Doppler lidar scans were successfully used to study the horizontal wind field and structures in the ABL over urban flat terrain for short time periods of a few hours (NEWSOM et al., 2005; NEWSOM et al., 2008). TRÄUMNER et al. (2015) used dual-Doppler lidar measurements over flat horizontally heterogeneous terrain to statistically investigate turbulent structures and coherence in the horizontal wind field in the surface layer for a time period of around 300 h. They calculated stream- and crosswise integral length scales and analyzed them for situations with different atmospheric stratification. A sequence of coplanar RHI and PPI scans performed with three scanning Doppler lidars was used by HAID et al. (2020) to study the interaction between a cold pool and foehn over the city of Innsbruck in the Inn Valley, Austria. From the three described configurations, coplanar horizontal scans provide the horizontal wind field with the highest spatial and temporal resolution, however at the expense of information on the vertical structure of the horizontal wind field.

Coplanar horizontal Doppler lidar measurements were conducted in Stuttgart in summer 2018 within the framework of the Urban Climate Under Change [UC]^2 program. The program aims to develop and evaluate a new building-resolving urban climate model for entire city regions and to test its practicability and usability in collaboration with stakeholders (SCHERER et al., 2019b). To this purpose, high-quality three-dimensional observational data were collected in three major German cities, one of them being Stuttgart (SCHERER et al., 2019a). Stuttgart is a city in moderate mountainous terrain in south-western Germany which frequently suffers from air quality issues. The orography is characterized by a basin-shaped valley (Stuttgart basin) which opens into the Neckar Valley in the north-east (Figure 1a). This complex topography makes Stuttgart an excellent location in which to study the interactions between processes on different scales such as convection and thermally driven circulations. Using coplanar Doppler lidar measurements from 22 days in July and August 2018 together with additional in situ and remote sensing data, the following research questions are addressed in this study:

1. Which mesoscale horizontal flow structures occur in the area characterized by the opening of the Stuttgart basin and the Neckar Valley? How regularly do these structures occur? How do they depend on atmospheric stratification and the wind above the mean ridge height?
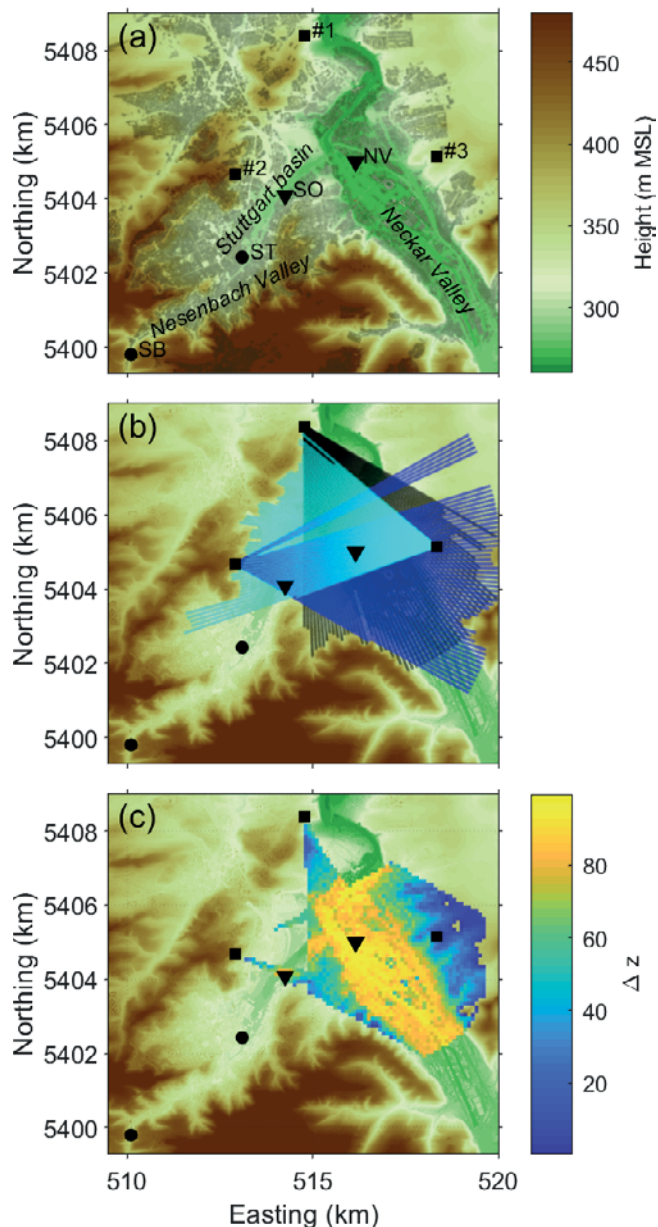
Figure 1: (a) Topographic height (terrain plus building height) in the investigation area with instrument locations. Buildings within the city limits of Stuttgart are indicated in gray. Squares indicate the locations of the scanning lidars #1, #2 and #3, respectively; circles mark the location of the surface station in Böblingerstraße in the Nesenbach Valley (SB) and the location of the town hall in the Stuttgart basin (ST); the triangles SO and NV indicate the points at the opening of the Stuttgart basin into the Neckar Valley and in the Neckar Valley, respectively, at which the retrieved horizontal wind field is analyzed in detail. (b) Topographic height and markers like in (a), but with the PPI sectors scanned by lidars #1 (black), #2 (blue) and #3 (cyan) taking into account beam blocking by the topography. Each dot indicates one range gate. (c) Topographic height and markers like in (a), but with the distance Δz of the lidar scanning plane above the topography at each grid point of the Cartesian retrieval grid. Only grid points where the intersection angle criteria is fulfilled are displayed. Coordinate system: UTM (ETRS89) zone 32U.

2. Is it possible to trace convective cells in the convective ABL over complex terrain and to estimate the convection velocity using coplanar Doppler lidar measurements? How does the convection velocity relate to the mean horizontal wind speed?

The paper is outlined as follows: in Section 2, the investigation area, instrumentation and the method to retrieve the horizontal wind field are described. Section 3 gives examples of the flow characteristics and Section 4 contains a statistical analysis of the mesoscale flow structures including the dependency on the ambient conditions. In Section 5, the displacement of convective cells is investigated and the method to derive the convection velocity is described. A summary and conclusions are given in Section 6.

2 Measurement setup and data processing

2.1 Investigation area

The investigation area in Stuttgart is characterized by a basin-shaped valley called Stuttgart basin with a horizontal dimension of around $3\,\mathrm{km} \times 3\,\mathrm{km}$ (Figure 1a). The Stuttgart downtown area is located in this basin. In the south-west, the basin is joined by the Nesenbach Valley and in the north-east, it opens into the Neckar Valley. The Neckar Valley roughly extends from the south-east to the north-west and is around $2\,\mathrm{km}$ wide. Besides these main characteristics, several smaller-scale orographic features such as side valleys and plateaus exist in the area. The mean height of the surrounding ridges is at around $520\,\mathrm{m}$ above mean sea level (MSL) which is about 170 to $270\,\mathrm{m}$ above the valley floor. The Stuttgart basin and the Neckar Valley are both heavily built-up with residential and industrial areas. The local summer time in Stuttgart is UTC plus $2\,\mathrm{h}$ and mean sunrise and sunset during the investigated period (21–29 July 2018, 16–28 Aug 2018) are at around 04:10 UTC and 18:45 UTC, respectively. In July and August 2018, five remote sensing devices, all part of the mobile observation platform KITcube operated by Karlsruhe Institute of Technology (KALTHOFF et al., 2013), were deployed in the area (KISELEVA et al., 2019).

2.2 Coplanar Doppler lidar measurements and retrieval of the horizontal wind field

In order to use coplanar horizontal Doppler lidar scans to study the spatio-temporal variability of the flow field, strict conditions and requirements must be met by the experimental setup. Ideally, the lidars should be installed at the same height above mean sea level, have an unobstructed view of the overlapping area and perform the PPIs at 0° elevation angle, which has the advantage that the measured radial velocity is purely a projection of the horizontal wind without any contributions by the vertical wind. The range gate lengths of the individual lidars, the

angular resolution of the PPI scans and the spacing of the grid on which the horizontal wind field is evaluated have to be fine enough to resolve the required spatial scales. The lidars have to perform synchronized sweeps, i.e. they have to start and stop each PPI at the same time, and the time required for each PPI scan has to be short enough to capture the temporal variability of the flow field.

These requirements were taken into account when installing three Doppler lidars "Windcube 200s" manufactured by Leosphere in Stuttgart. They were placed on three opposing slopes (Figure 1a): lidar #1 (363 m MSL) was installed on the grounds of the German Weather Service (DWD) at Schnarrenberg, lidar #2 (381 m MSL) in a vineyard owned by the city of Stuttgart and lidar #3 (351 m MSL) on the grounds of the wine estate Wöhrwag. Due to the challenge to find suitable measurements sites, the lidars were not all at exactly the same height above sea level, but had an offset of up to 30 m. The average height of the scanned plane was defined as 365 m MSL, which is on average about 62 m above the underlying topography (Figure 1c) and about half way up the slopes. The sectors of the conducted PPI scans were limited by the topography, which e.g. prevented lidar #1 to scan at azimuth angles larger than 180° (Figure 1b). All three lidars are identical in construction and were operated with the same technical specifications. A physical range gate resolution of 50 m (laser pulse length 200 ns) and no overlapping range gates resulted in a maximum theoretical measurement range of 100 to 7200 m with 143 range gates. The accumulation time was set to 1 s and each PPI scan lasted for 60 s. As the azimuth sector was 60° for all lidars, the angular resolution was 1°. The PPI scans were started synchronously every minute for all three lidars using the "Scheduler" option of the manufacturer software "Windforge" (version 3.1.1). The synchronization accuracy of the start times was around 0.35 s on average for all investigated days.

Every minute, a set of three horizontal PPI scans was obtained, which is used for the retrieval of the horizontal wind field. At 0° elevation angle, the radial velocity, rv, measured by a Doppler lidar is a projection of the two-dimensional horizontal wind vector, $v_h = (u, v)^T$:

$$rv = \hat{r} \cdot v_h = u \sin(az) + v \cos(az) \qquad (2.1)$$

with the two-dimensional unit vector in the direction of the lidar beam, $\hat{r}$, and the azimuth angle, az. In order to solve Eq. 2.1, at least two radial velocity measurements at the same point in space and time with different azimuth angles have to be available. The radial velocity measurements from the PPI scans are neither perfectly simultaneous nor exactly collocated. Because of this, the horizontal wind vector is retrieved on a Cartesian grid with a lattice length $\Delta l = 100$ m spanning the horizontal scanning plane. The maximum temporal offset at an arbitrary grid point is given by the scan duration of 60 s. To each grid point of the Cartesian grid, radial velocity measurement values from all three lidars

are assigned within a certain radius $R = \Delta l / \sqrt{2}$ of the grid point and the intersection angle of the individual lidar beams is calculated. A system of N linear equations results at each grid point, with N being the number of radial velocity measurement values that fall within R. This system is solved by minimizing its cost function

$$J = \sum_{n=1}^{N} (rv_n - \hat{r}_n \cdot v_h)^2 \qquad (2.2)$$

and the most probable horizontal wind components are deduced. A more detailed description of the retrieval method is e.g. given by HAID et al. (2020) and the Python code of the algorithm is available at GitHub (HAID, 2019). Before solving Eq. 2.2, the radial velocity measurements are filtered for outliers applying a threshold filter to the carrier-to-noise ratio of -30 dB and a velocity jump filter of $2 \, \text{m s}^{-1}$ to identify rapid, unrealistic changes at each range gate for successive time stamps (1 s increments). The horizontal wind components are rejected for grid points which do not fulfill the intersection angle criteria: the intersection angle has to be between 30° and 150° for at least two of the lidars to avoid too large propagation errors, following the suggestions and considerations by STAWIARSKI et al. (2013) and TRÄUMNER et al. (2015). The largest possible area at which the horizontal wind field can be retrieved covers several square kilometers (about 5 km × 5 km) (Figure 1c). The constraints by the intersection angle prevent the retrieval in a substantial part of the opening of the Stuttgart basin into the Neckar Valley. The area is further limited by the actual measurement ranges of the lidars, which is usually lower during the day than during the night, as visible in the horizontal wind field examples in Figure 2. The larger measurement ranges during the night could be related to higher backscatter due to a higher aerosol concentration when pollutants get trapped within the nocturnal surface inversion layer or due to higher relative humidity values during nighttime resulting in the growth of hygroscopic aerosols (e.g. VESELOVSKII et al., 2009).

2.3 Additional instrumentation

In addition to the scanning "Windcube 200s" Doppler lidars, a fourth vertically profiling Doppler lidar "Windcube WLS8-3" also manufactured by Leosphere was installed on the roof top of the town hall (ST in Figure 1a) at 325 m MSL in the Stuttgart basin. It provided horizontal wind profiles with the Doppler beam swinging (DBS) technique in a vertical range between 40 to 600 m above the device with an averaging interval of 10 min. The DBS technique is based on the assumption of horizontal homogeneity which may not be given over complex terrain. This can induce errors in the horizontal wind speed in the order of 10 % (BINGÖL et al., 2009).

Information on the atmospheric stratification was obtained with a microwave radiometer "HATPRO-G4" manufactured by Radiometer Physics GmbH, which was
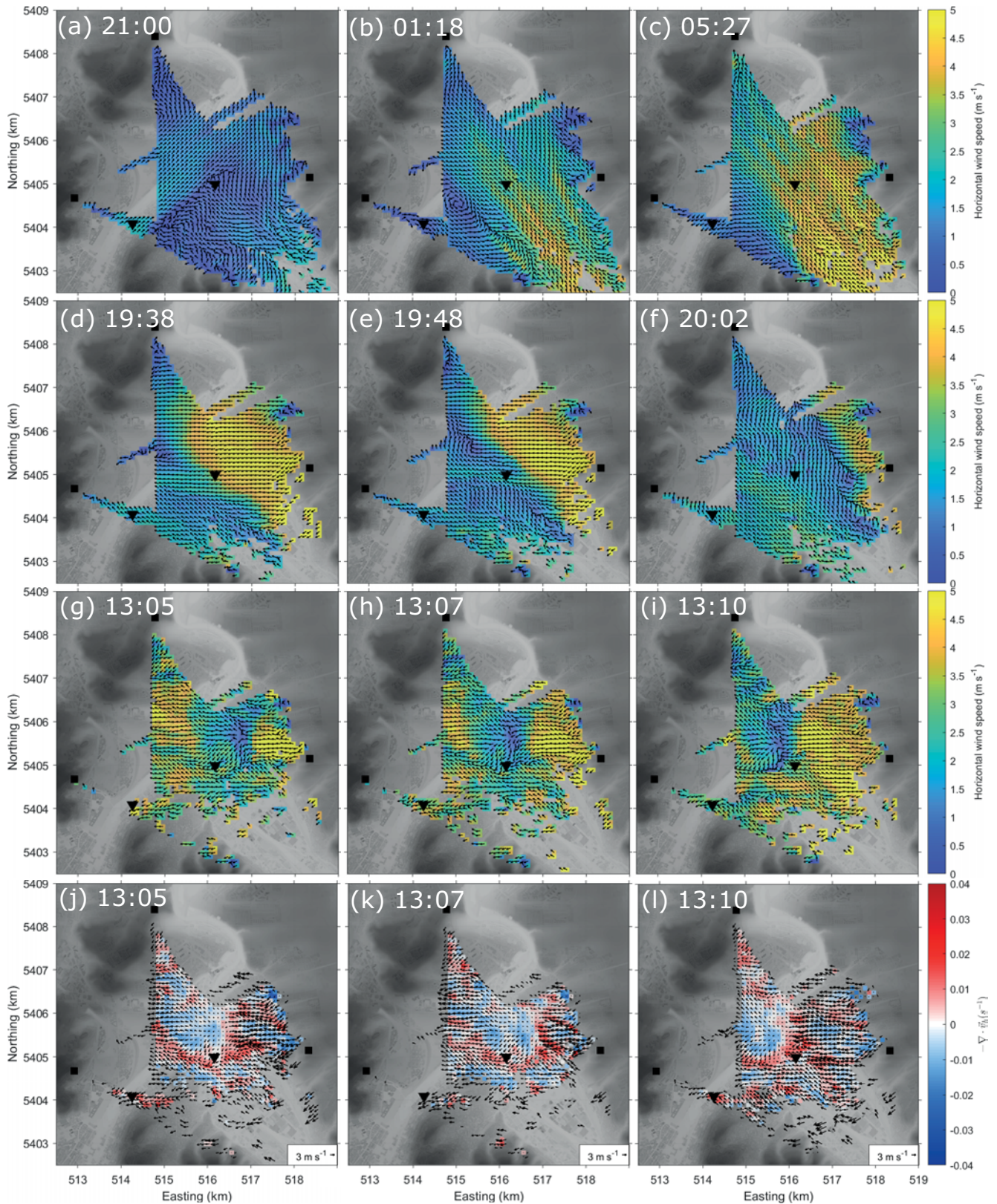
Figure 2: Examples of horizontal wind fields observed during different periods: horizontal wind speed (color-coded) and vector (arrows) during nocturnal stable conditions at (a) 21:00 UTC, (b) 01:18 UTC and (c) 05:27 UTC; during the transition between convective and stable conditions at (d) 19:38 UTC, (e) 19:48 UTC and (f) 20:02 UTC; and during daytime convective conditions at (g) 13:05 UTC, (h) 13:07 UTC and (i) 13:10 UTC. The horizontal divergence fields corresponding to the horizontal wind fields shown in (g)–(i) is displayed in (j)–(l). The example in (a) is on 23 July, the examples in (b)–(l) are on 24 July. Grey shading shows the topographic height, squares indicate the locations of lidars #1, #2 and #3 and the triangles mark the points SO and NV, respectively (see Figure 1a).

installed on the tower of the town hall (ST in Figure 1a) at 357 m MSL in the Stuttgart basin. The retrievals to obtain temperature profiles from the measured brightness temperature are created with software provided by the University of Cologne (LÖHNERT and CREWELL, 2003; LÖHNERT et al., 2009) and are based on nearly 20.000 radiosoundings performed at the DWD observatory at Schnarrenberg twice a day. By adding information from low-elevation boundary-layer scans performed every 15 min the accuracy of the temperature profiles in the ABL was enhanced (CREWELL and LÖHNERT, 2007). Due to the position of the microwave radiometer, the boundary-layer scans were performed over the buildings within the Stuttgart basin. Thus, the retrieved temperature values start around 60 m above the valley floor and represent an average over the conditions in the basin. Using the air pressure measurements at the device's housing, potential temperature profiles are calculated.

Wind measurements with a cup anemometer and a wind vane at 10 m above ground were conducted at a surface station in Böblingerstraße in the Nesenbach Valley (SB in Figure 1a) at 356 m MSL, which was operated by DWD.

3 Examples of horizontal flow characteristics

In this section, we demonstrate the potential and possibilities of the retrieved horizontal wind fields for the study of boundary-layer flow characteristics. Using the example of a 24-hour period (21:00 UTC 23 July to 21:00 UTC 24 July) with fair weather conditions and a weak ($<5\,\mathrm{m\,s^{-1}}$) large-scale easterly wind, we illustrate the characteristics of the horizontal flow field at different times of the day. A 24-h movie of the horizontal flow field is available as supplementary information (ADLER et al., 2020). The overall flow characteristics during this period are typical and occur frequently on the investigated days, which will be shown in Sections 4 and 5.

In the evening before a strong south-easterly downvalley wind in the Neckar Valley is established, southwesterly flow at the opening from the Stuttgart basin into the Neckar Valley indicates an outflow of the basin of around 2 m s^{-1} (Figure 2a). A few hours later, the southeasterly downvalley wind in the Neckar Valley has increased in strength. A weak outflow of the basin is still visible and a counter-clockwise vortex is detected in the area between the outflow and the downvalley wind (Figure 2b). In the early morning, a strong ($\approx 5\,\mathrm{m\,s^{-1}}$) southeasterly downvalley wind in the Neckar Valley exists and an inflow into the basin is observed at the opening (Figure 2c). Towards the slopes where the distance between the lidar scanning plane and the underlying terrain is smaller (Figure 1c), the downvalley wind is weaker or even not visible (Figure 2b, c).

Another interesting flow feature is observed in the evening towards the end of the example period (Figure 2d–f). In the western part of the Neckar Valley, the horizontal wind is rather weak ($<1.5\,\mathrm{m\,s^{-1}}$) from southeasterly direction, i.e. downvalley, while it is easterly with values of more than 5 m s^{-1} in the eastern part (Figure 2d). In between, horizontal convergence exists. Over a period of around 20 min, the area with easterly wind becomes smaller and only exists over the eastern most part of the Neckar Valley at 20:02 UTC (Figure 2d–f). At the same time, the downvalley wind in the Neckar Valley becomes stronger (up to 3 m s^{-1}) and spreads out. The flow feature is not further investigated in this study, but it could make an interesting case to be studied in a combined observational and numerical analysis. We think that this feature could be related to the following processes: due to longer-lasting insolation on the eastern slopes in the evening, the ABL in the eastern part is less stably stratified than in the western part. While the flow is still coupled to the ambient easterly wind in the eastern part, a downvalley wind already forms in the western part. As the ABL becomes more and more stably stratified over time, the coupling weakens and eventually downvalley wind dominates in the whole valley. Another possible explanation is the formation of a wave over the terrain east of the Neckar Valley, which penetrates into the eastern part of the Neckar Valley as long as the stratification in the valley is not too stable. When the static stability in the ABL becomes stronger the penetration is inhibited, similar to the situation when a cold pool filling a valley inhibits the penetration or breakthrough of foehn down to the surface (HAID et al., 2020).

While the flow features described above occur on the scale of the valleys, i.e. on the mesoscale, sub-mesoscale structures are visible during daytime on many of the 22 investigated days. These structures present themselves as areas of enhanced or reduced horizontal wind speed associated with horizontal divergence and convergence, as exemplary shown in Figure 2g–l. They are similar to coherent structures detected by TRÄUMNER et al. (2015) in the surface layer over flat terrain using dual-Doppler lidar measurements. These authors found that the shape and size of the structures depend on stratification and horizontal wind speed. In the example in Figure 2g-i, the displacement of an area with reduced horizontal wind speed can be tracked in the horizontal wind field images over a time period of 5 min. The structure moves from east to west from around 517 km to 515.5 km Easting. This structure strongly resembles open-cell convection reported by TRÄUMNER et al. (2015) on calm days and we thus assume that the detected enclosed structure is related to a convective cell. We estimate the convection velocity from the movement of the cell (around 1.5 km in 5 min) to be around 5 m s^{-1}. During convective periods, no clear impact of the terrain on the flow is visible which can be seen in the 24-h movie in the supplementary information (ADLER et al., 2020).
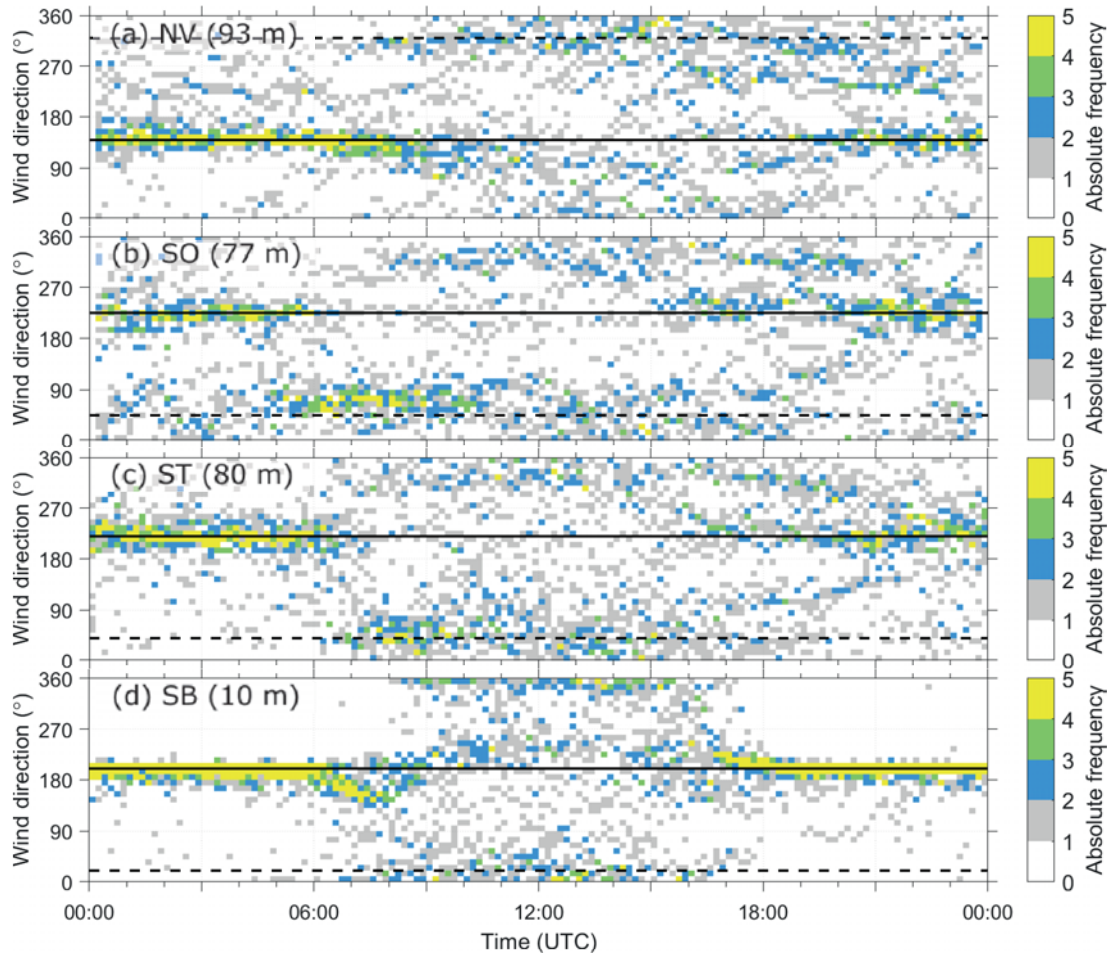
Meteorol. Z. (Contrib. Atm. Sci.)
PrePub Article, 2020

B. Adler et al.: Structures in the horizontal wind field over complex terrain

7

Figure 3: Time series of the absolute frequency distribution (number of days for which the wind direction is within a $10\,\text{min} \times 10°$ bin) of the wind direction below the mean ridge height in (a) the Neckar Valley (NV), (b) the opening of the Stuttgart basin (SO), (c) the Stuttgart basin (ST) and (d) the Nesenbach Valley (SB) based on the horizontal wind data of all 22 available days. The height above the topography at which the measurements were taken are indicated in brackets. To make the wind directions at NV and SO, which are retrieved from the coplanar Doppler lidar scans, comparable to the data from the wind profiling lidar (ST) and the surface station (SB), the wind direction at NV and SO are averaged over 10 min before calculating the frequency distribution. Dashed and solid lines indicate up- and downvalley direction in (a), (c) and (d) and in- and outflow direction in (b), respectively.

4 Statistics of mesoscale flow structures

4.1 Frequency distribution of the wind direction

The individual horizontal wind fields (Figure 2) from the example in Section 3 indicate that different types of flow regimes occur on the mesoscale depending on the time of the day and location. To get a statistical view of the flow conditions below the mean ridge height, the horizontal wind direction is evaluated at four locations: one in the Neckar Valley (NV in Figure 1a) and one in the opening of the Stuttgart basin into the Neckar Valley (SO). In addition, the horizontal wind direction at 405 m MSL measured with the profiling lidar on the roof top of the town hall in the Stuttgart basin (ST) and at the surface station at Böblingerstraße (SB) is analyzed statistically to extend the investigation of the flow characteristics into the Stuttgart basin and the Nesenbach Valley. The measurement height at the locations in the

Neckar Valley, at the opening and in the Stuttgart basin was around 80–90 m above the underlying topography, while the measurements in the Nesenbach Valley were taken at 10 m above the ground. This means that all measurements were taken well below the mean ridge height. The absolute frequency distribution of the wind direction at the four locations is calculated for all 22 days (Figure 3).

From the late morning until the early evening, the wind direction is rather scattered at all locations, with a slight preference for a northerly flow component (Figure 3).

During the night and morning hours, distinct differences are evident at the individual sites, which are inline with the orographic structures. In the northwest-southeast oriented Neckar Valley (Figure 3a), south-easterly flow clearly dominated during nighttime and in the early morning until around 08:30 UTC, which corresponds to a downvalley wind. In the Stuttgart basin (Figure 3c) and in the Nesenbach Valley (Fig-

ure 3d), the dominant wind direction during the night (around 20:00 UTC to 06:00 UTC) is south-westerly and southerly, respectively. This indicates downvalley wind flowing out of the Nesenbach Valley into the Stuttgart basin following the shape of the terrain (Figure 1a).

At the opening of the Stuttgart basin into the Neckar Valley, two wind directions prevail during the night and morning hours (Figure 3b): from around 20:30 to 05:00 UTC south-westerly flow dominates, indicating an outflow of the basin into the Neckar Valley. After around 05:00, north-easterly flow becomes more prominent, which is equivalent with an inflow into the basin from the Neckar Valley. The flow field in Figure 2c is an example for such a flow condition from which it seems likely that the inflow into the basin is related to the downvalley wind in the Neckar Valley which pushes through the opening into the basin.

4.2 Dependency of the flow below the mean ridge height on the flow aloft and atmospheric stratification

In the next step, the relationship between the wind direction below the mean ridge height at three different locations (in the Stuttgart basin (ST), at the opening (SO) and in the Neckar Valley (NV)) and the wind direction above the mean ridge height and atmospheric stratification is investigated. We follow the approach described by WITTKAMP et al. (submitted) who investigated the same relationship during summer 2017. Instead of using coplanar horizontal scans, these authors retrieved wind direction profiles at the opening of the Stuttgart basin and in the Neckar Valley with the virtual tower method. In our study, the ambient horizontal wind, i.e. the wind above the mean ridge height, is defined as the horizontal wind measured at 705 m MSL with the profiling lidar and the Bulk-Richardson number (BRN) is calculated using horizontal wind and temperature information at two heights (405 and 685 m MSL) from the profiling lidar and the microwave radiometer located at ST in the Stuttgart basin. WITTKAMP et al. (submitted) found a critical BRN value of 1.25 which separated dynamically unstable cases (BRN < 1.25), during which the flow in the valleys was coupled to the flow aloft and dynamically stable cases (BRN > 1.25), during which the flow was decoupled and mainly directed in downvalley direction. In our study, around 2500 10-min periods are available for the analysis during the 22 investigated days, which are nearly equally distributed over three BRN regimes, i.e. BRN < 0, $0 \leq$ BRN < 1.25, BRN $\geq$ 1.25. Our sample size is thus much larger than the one available during summer 2017 and presented in WITTKAMP et al. (submitted).

During convective conditions (BRN < 0), wind direction below and above the mean ridge height match, i.e. the values lie on or near the diagonal for many of the cases (Figure 4a, d, g). During dynamically unstable conditions ($0 \leq$ BRN < 1.25), wind direction below and above the mean ridge height are also often similar

when the wind above the mean ridge height comes from the south-westerly to north-westerly sector, i.e. 250° and 330° (Figure 4b, e, h). For these cases, the wind direction below ridge is slightly turned counter-clockwise, i.e. the values lie below the diagonal. Independent of the wind direction above the mean ridge height, south-easterly downvalley wind is another common wind direction in the Neckar Valley for this stability regime (Figure 4b). This means that the flow in the valley is decoupled from the flow aloft, although the BRN values indicate dynamically unstable conditions. Due to the orientation of the valley axis in the Stuttgart basin, it is not possible to make this distinction in the Stuttgart basin (Figure 4h). For BRN > 1.25, i.e. dynamically stable conditions, the flows in the Neckar Valley (Figure 4c) and in the Stuttgart basin (Figure 4i) have a clear preference for downvalley direction, i.e. south-easterly in the Neckar Valley and south-westerly in the Stuttgart basin.

At the opening of the Stuttgart basin, the preferred wind directions during thermally stable conditions are north-easterly, which indicates an inflow, and south-westerly, which indicates an outflow (Figure 3e, f). The two flow regimes are most pronounced during dynamically stable conditions (Figure 3f).

4.3 Discussion and interpretation

During convective conditions the wind direction below and above the mean ridge height are similar at all sites (Figure 4a, d, g), which indicates that both layers are coupled due to turbulent mixing in the convective ABL. A slight preference for a northerly flow component is visible (Figs. 3 and 4a, d, g). Given the orientation of the valleys (Figure 1a), north-westerly flow in the Neckar Valley (Figure 3a), north-easterly flow in the Stuttgart basin (Figure 3c) and northerly flow in the Nesenbach Valley (Figure 3d) indicate upvalley wind. Besides the upvalley wind, south-westerly wind sometimes occurs in the Nesenbach Valley during the day (Figure 3d) which could be related to large-scale driven channeling (WHITEMAN and DORAN, 1993). The slightly counter-clockwise turned wind direction below the mean ridge height for dynamically unstable conditions (Figure 4b,e,h) could be related to the impact of surface friction on the flow below the mean ridge height, which becomes relevant as vertical mixing is lower in this regime than during convective conditions. This is in agreement with the Ekman spiral theory (e.g. STULL, 1988) and is also found by WITTKAMP et al. (submitted).

Cases with coupled flows (wind direction below and above the mean ridge height are similar) and uncoupled flows (downvalley wind independent of the wind direction above the mean ridge height) are both found in the Neckar Valley for dynamically unstable conditions (Figure 4b). Both cases are scattered throughout the whole range of BRN values (between 0 and 1.25). This means that changing the BRN thresholds to define the dynamically unstable regime does not allow to better distinguish between both cases. One possible reason for this
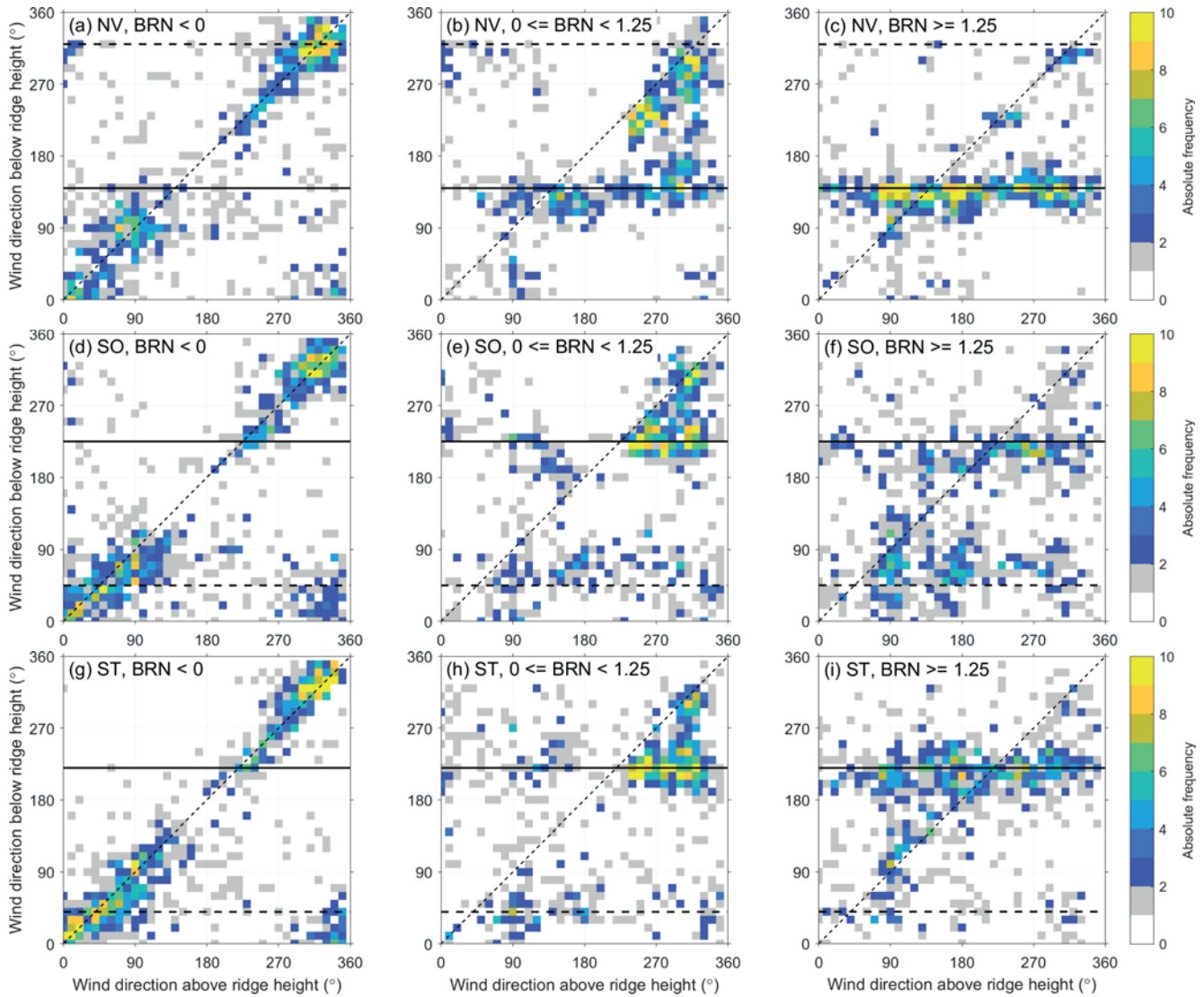
Meteorol. Z. (Contrib. Atm. Sci.)
PrePub Article, 2020

B. Adler et al.: Structures in the horizontal wind field over complex terrain

9

Figure 4: Relationship between the wind direction above the mean ridge height at 705 m MSL and the wind direction below the mean ridge height at 365 m MSL in (a, b, c) the Neckar Valley (NV) and (d, e, f) the opening of the Stuttgart basin (SO) and at 405 m MSL (g, h, i) in the Stuttgart basin (ST). The data are separated according to the BRN regimes: (a, d, g) BRN < 0, (b, e, h) $0 \le$ BRN < 1.25 and (c, f, i) BRN ≥ 1.25. The color code shows the number of days for which the wind direction is within a $10° \times 10°$ bin. The wind components at NV and SO, which are retrieved from the coplanar Doppler lidar scans, are averaged over 10-min periods before calculating the wind direction. Dashed and solid horizontal lines indicate up- and downvalley direction at NV and ST and in- and outflow direction at SO, respectively.

could be that the conditions in the Stuttgart basin, where BRN is calculated, are not representative for the conditions in the Neckar Valley during these cases. Another reason could be the uncertainty related to the BRN calculation as both the temperature profiles measured by the microwave radiometer and the horizontal wind profiles from the profiling lidar are subject to errors related to the measurement techniques.

Based on the BRN values, it is not possible to distinguish between inflow and outflow cases at the opening of the Stuttgart basin (Figure 4e, f). This could be related to the same reasons as above, i.e. the non-representativity of the BRN values for the conditions at the opening and the uncertainty of the BRN calculation. The diurnal cycle of wind direction at the opening (Figure 3b), however, indicates that an outflow is more likely dur-

ing nighttime and an inflow preferentially occurs during the morning hours. There is no clear dependency of both flow regimes on the wind direction above ridge level, although a slight preference of outflow with ambient westerly wind might exist (Figure 4e, f).

5 Displacement of structures in the convective ABL

During daytime, the movement of structures characterized by enhanced and reduced horizontal wind speed is often detected on the 22 investigated days (example in Figure 2g–i) and we relate these structures to convective cells which move through the ABL with a certain convection velocity. Sophisticated methods to track

structures in time and space have been developed in the past (e.g. HANDWERKER, 2002). Based on the calculation of the spatial cross-correlation between subsequent images of the horizontal wind field, DUNCAN JR et al. (2019) proposes a method to estimate the speed with which structures move downwind. However, their method relies on a well resolved wind field and a large data availability within the measurement domain. Data availability during daytime is often limited by the maximum measurement ranges of the lidars during daytime, which may lead to only partial resolution of the convective cells. Such a method based on the spatial cross-correlation is thus not applicable to our data.

5.1   Method to estimate the convection velocity

To estimate the convection velocity, we therefore use the following method which works well with the imposed restrictions. We first estimate the mean wind direction for a 60-min period by temporally and spatially averaging the horizontal wind components. Figure 5a shows an example of the spatial distribution of the temporally averaged horizontal wind field. A line along the mean wind direction is then placed through the location in the Neckar Valley (NV). This location was chosen as it was often near the center of the area where the horizontal wind retrieval provided data. For every individual horizontal wind field within the 60-min period, the horizontal wind speed values along this line are extracted. An example of the resulting time distance plot of horizontal wind speed is shown in Figure 5b. To enhance the number of 60-min periods available for the analysis, gaps of less than 10 pixels (size of one pixel is $100 \, \text{m} \times 100 \, \text{m}$) in the time distance plots are linearly interpolated. For example, one pixel missing for 10 min or a gap of 1000 m during one time stamp are interpolated. The number of interpolated pixels is less than 1 % on the average. The displacement of structures with time is clearly visible as the elongated streaks with low and high horizontal wind speed. The slope of each streak represents the convection velocity of the corresponding cell. Instead of calculating the slope of each streak manually by hand, we estimate a global convection velocity for the 60-min period. To this purpose, the two-dimensional auto-correlation function is calculated for the 60-min time distance plot (Figure 5b, 6). From the slope a of the fit

$$l_t = a \cdot l_d \quad (5.1)$$

to the elongated shape of positive auto-correlation the convection velocity v_c is estimated as

$$v_c = |a|^{-1} \quad (5.2)$$

using only pixels where the auto-correlation function is larger than 0.5. l_t denotes the lag in time and l_d the lag in distance. This method can also be applied to radial velocity measured by a single lidar when the beam is pointed in the mean wind direction. This was e.g.
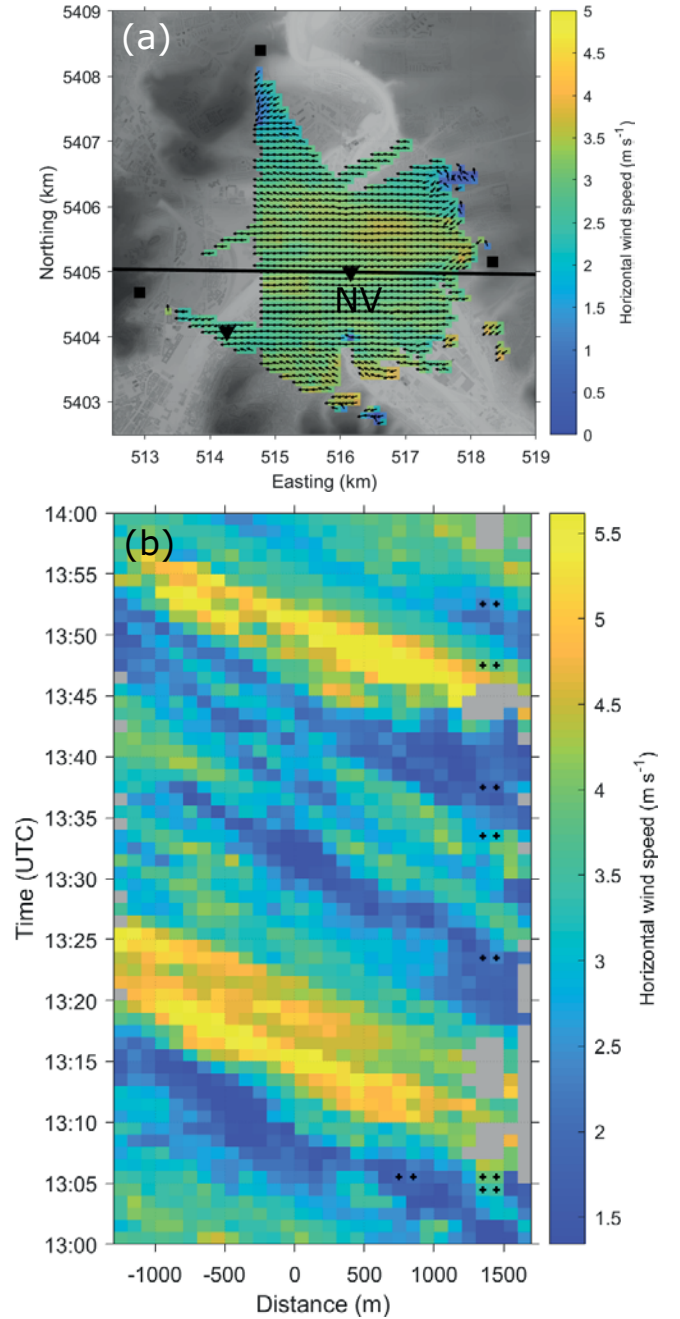

Figure 5: (a) Mean horizontal wind field averaged for the time period 13:00 to 14:00 UTC on 24 July. The black straight line indicates the mean wind direction of 91° which results when averaging the wind components over space and time for the 60-min period. Grey shading shows the topographic height. (b) Time distance plot of the horizontal wind speed along the straight line from (a) through the location NV in the Neckar Valley for the corresponding time period. In (b), crosses indicate pixels where the values are linearly interpolated.

done by PANTILLON et al. (2020) who applied the two-dimensional auto-correlation function to a time distance plot of radial velocity measured by single lidar during rapid low-elevation RHI scans to investigate coherent structures related to cyclonic winter storms.

If the availability of data in the 60-min time distance plot is too small or the fit to the two-dimensional
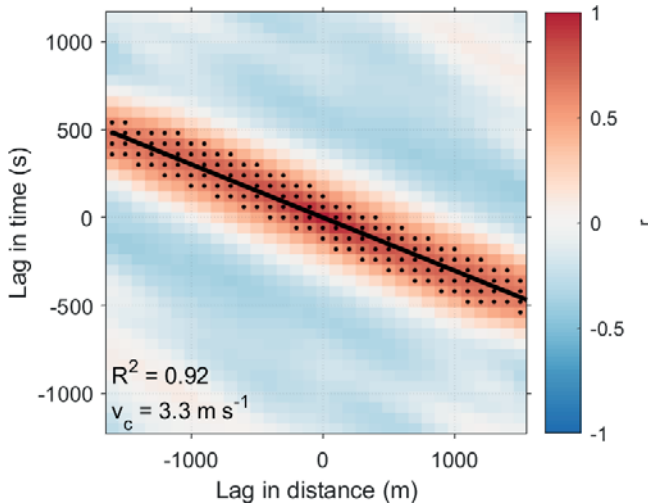
Meteorol. Z. (Contrib. Atm. Sci.)
PrePub Article, 2020

B. Adler et al.: Structures in the horizontal wind field over complex terrain

11

Figure 6: Two-dimensional auto-correlation function, r, of the time distance plot of the horizontal wind speed shown in Figure 5b. Only pixels with an auto-correlation larger than 0.5 (black dots) are used for the fit (black line). From the slope of the linear fit, the convection velocity, v_c, is determined if the coefficient of determination, R^2, is higher than 0.5.

auto-correlation function fails, the estimated convection velocity is not reasonable. Consequently, the convection velocity is disregarded when the dimensions of the horizontal wind speed field are less than 50×10 pixels, which corresponds to 50 min in time and 1000 m in space, or when the coefficient of determination of the fit is less than 0.5. Possible reasons for the fit to fail can be that simply no streaks are visible in the time distance plot as no convective cells propagate with the mean wind or that the wind direction changes substantially within the 60-min period.

5.2 Relationship between the horizontal wind speed and convection velocity

The method described in Section 5.1 is applied to all 22 days for the time period between 06:00 and 18:00 UTC. After applying the strict filter criteria, 83 60-min time periods remain. Figure 7a shows the relationship between the mean horizontal wind speed at 365 m MSL, i.e. at the height of the lidar scanning plane where the convection velocity is estimated, and the convection velocity. While both values generally agree quite well ($R^2 = 0.76$), the mean convection velocity is $0.6\,\mathrm{m\,s^{-1}}$ (24 %) higher than the mean horizontal wind speed, v_h, of $2.5\,\mathrm{m\,s^{-1}}$. The line of best fit is $v_h = 0.79 \cdot v_c$. This means that the cells move faster than the mean flow at the same height, which is in agreement with the findings of HAN et al. (2019). Note that this mean percentage value is quite sensitive to outliers. When excluding four values for which the difference between the wind speed and the convection velocity differed more than twice the standard deviation from the mean difference (values are indicated by the red outlines in Figure 7a) the mean convection velocity reduces

to $3.0\,\mathrm{m\,s^{-1}}$. As the mean horizonal wind speed stays the same, the convection velocity is then only 20 % higher than the mean wind speed.

It is rather likely that the movement of the cells is controlled by the horizontal wind speed in a certain height in the ABL. This steering level presumably depends on the vertical extent of the convective cells. Thus, individual cells may travel with a different speed, as they are steered by the flow at different levels depending on their vertical extent. With the method described in Section 5.1 we obtain a global convection velocity for all types of structures within each 60-min period, which does not take into account the movement of individual cells.

The lidar scanning plane is at 365 m MSL, i.e. 62 m above the topography on the average (Figure 1c). This means that it is still in the lower part of the ABL and probably in the transition zone between the surface layer and the mixed layer. As evident in the mean horizontal wind profile calculated for the corresponding periods from the profiling Doppler lidar in the Stuttgart basin, horizontal wind speed in the ABL increases with height up to around 600 m MSL and stays roughly constant above (not shown). This is likely due to the surface roughness induced by the buildings and terrain. The height at which the mean horizontal wind speed agrees with the mean convection velocity of $3.1\,\mathrm{m\,s^{-1}}$ is at around 465 m MSL, i.e. 100 m above the lidar scanning plane. Although the scatter is larger and the coefficient of determination is smaller ($R^2 = 0.51$) when comparing the convection velocity with the horizontal wind speed at 465 m MSL (Figure 7b) instead of at 365 m MSL (Figure 7a), it is evident that the values lie closer around the bisectrix (slope of the line of best fit is 0.95) in Figure 7b than in Figure 7a. This means that the speed with which the convective cells detected at 365 m MSL overall move is closer to the horizontal wind speed at 465 m MSL, i.e. the cells movement is steered by the flow at this higher level. The larger scatter in Figure 7b than in Figure 7a could be related to the uncertainties related to the horizontal wind measurements by the profiling lidar and to the spatial distance of a few kilometers between the profiling lidar measurements in the Stuttgart basin and the coplanar lidar measurements in the Neckar Valley (Figure 1).

6 Summary and conclusions

The flow in the ABL over complex terrain is highly variable in space and time. In order to capture the (sub-) mesoscale characteristics of the flow by means of observations, simultaneous measurements at many locations in space are necessary. In some distance above the surface or in complex or inaccessible terrain such as urban or mountainous areas, these kind of measurements can realistically only be obtained with remote sensing instruments. By performing synchronized horizontal coplanar scans with three Doppler lidars on 22 days in
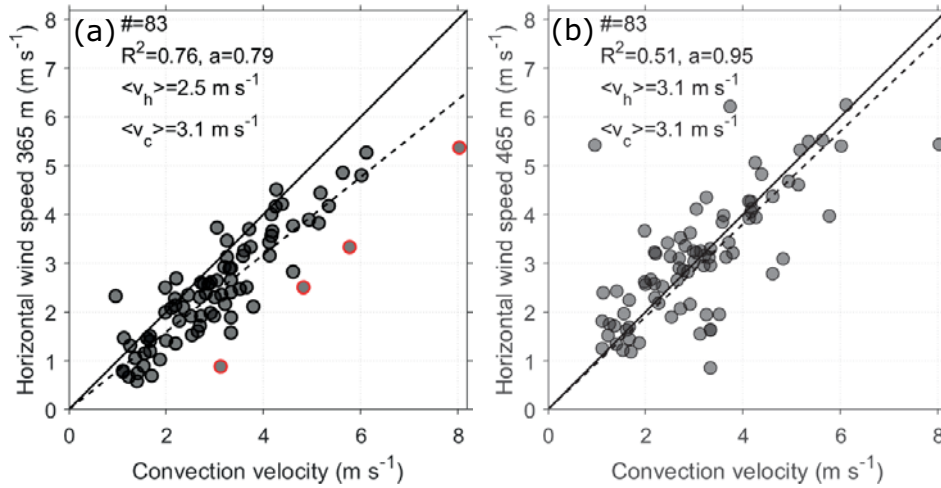
Figure 7: Relationship between the convection velocity and (a) the mean horizontal wind speed at 365 m MSL determined from the temporal and spatial average of the retrieved horizontal wind components for each 60-min period and (b) the horizontal wind speed at 465 m MSL measured by the profiling lidar at ST. The convection velocity is estimated with the method described in Section 5. The solid line indicates the bisectrix and the dashed line shows the line of best fit, $v_h = a \cdot v_c$. The coefficient of determination, R^2, the slope of the line of best fit, a, the mean horizontal wind speed, $\langle v_h \rangle$, and the mean convection velocity, $\langle v_c \rangle$ are given. The red outlines in (a) indicate outlier values (for details see text).

summer 2018 within the $[UC]^2$ program, we retrieved the horizontal wind field in a horizontal plane of several square kilometers above the city of Stuttgart. The terrain around Stuttgart is characterized by a basin-shaped valley (Stuttgart basin) which is joined by the Nesenbach Valley and opens into the larger Neckar Valley. The horizontal wind field is available every 60 s and has a horizontal resolution of 100 m. This study pursues two main objectives: (1) to identify the mesoscale flow structures in the valleys and to investigate how often they occur and how they depend on the flow above the mean ridge height and on atmospheric stratification and (2) to detect and trace convective cells which move through the ABL and to estimate the convection velocity.

1. During dynamically stable conditions, which are identified by calculating the Bulk-Richardson number, the flow below the mean ridge height is regularly decoupled from the flow aloft and the wind direction in the Neckar Valley, Nesenbach Valley and Stuttgart basin reveals a clear preference for thermally driven downvalley wind. At the opening of the Stuttgart basin into the Neckar Valley, two flow regimes are found, which are rather independent of the wind direction above the mean ridge height. An outflow of the basin occurs mainly during the nighttime hours, while an inflow dominates in the morning. The switching between in- and outflow may have important implications for the ventilation of the Stuttgart basin and thus for the air-quality, which will be investigated in future studies.

   During thermally unstable conditions, the flow below and above the mean ridge height is mainly coupled, i.e. the wind direction is very similar. Although the wind direction varies a lot, a preference for northerly flow is evident, which is equivalent to upvalley wind.

The large spread is likely related to the moderate valley depths of around 200 m in which thermally driven circulations are less pronounced and masked during daytime by convection compared to deeper valleys.

2. Convective cells which propagate downstream are detected during daytime in the horizontal wind field. When plotting the horizontal wind speed extracted along the line of the mean wind direction against time for 60-min periods, elongated streaks are visible. The slope of each streak gives the speed with which the cell propagates downstream, i.e. the convection velocity. This velocity is relevant when temporal point measurements are transferred to space to investigate the spatial characteristics of the cells. By calculating the two-dimensional auto-correlation function for each 60-min time distance plot, a global convection velocity is obtained for all cells within each time period. Comparing the convection velocity with the mean horizontal wind speed at the height of the lidar scanning plane at 365 m MSL (about 62 m above the topography), i.e. the same level where the convection velocity is calculated, reveals that the correlation between both velocities is quite good ($R^2 = 0.76$), while the convection velocity is higher by 24 % on the average. This result, which is retrieved from measurements over highly complex urban and mountainous terrain, is in general agreement with the findings of HAN et al. (2019), whose results are based on tower measurements conducted over a dry flat bed of a lake.

   Using horizontal wind profiles obtained with a profiling lidar in the Stuttgart basin a few kilometers away from the area where the convection velocity is estimated, we find that the global convection ve-

Meteorol. Z. (Contrib. Atm. Sci.)
PrePub Article, 2020

B. Adler et al.: Structures in the horizontal wind field over complex terrain

13

locity is more similar to the horizontal wind speed 100 m above the lidar scanning plane. This suggests that this is the overall steering level, which controls the movement of the convective cells. This could be further investigated with an experimental setup consisting of profiling measurements in the area of the coplanar horizontal scans and several sets of scanning lidars which are installed at different heights on slopes overlooking a valley deeper than the one targeted here. This would allow to retrieve the convection velocity at several levels throughout the ABL. Such a setup might also give new insights into the spatial characteristics of the flow in deeper valleys. The vertical cross-valley flow structure in such valleys has recently been targeted by vertical coplanar Doppler lidar measurements in the Inn Valley, Austria, (ADLER et al., submitted), but detailed measurements of the horizontal flow structure with high spatio-temporal resolution are still missing.

Our analysis demonstrates the benefit of area-wide measurements of the horizontal wind field with a high spatial and temporal resolution in contrast to point measurements at individual sites which suffer from limited representativeness in complex terrain. This kind of information can only be achieved by measuring simultaneously at the same point in space with at least two Doppler lidars. The third Doppler lidar used in this study enlarges the area in which the horizontal wind field can be retrieved. With such spatial measurements it is e.g. possible to detect and study the spatial variability and diurnal cycle of the flow within a valley or at the confluence of two valleys which is influenced by the interaction of convection and thermally and dynamically driven flows. Even vortices with a vertical axis or convective cells can be visualized. One big issue when performing point measurements at towers or with a profiling lidar is often the representativity of the location. Spatial measurements performed with coplanar Doppler lidar scans could help to address the representativity and to identify suitable locations. These types of measurements also open up new possibilities for model evaluation and may prove useful for air pollution studies and wind energy research. In future scenarios when drones are flying over cities e.g. to deliver medicine or to monitor traffic (KHAN et al., 2018), real-time monitoring of the wind field above cities, similar to the automatic wind shear detection performed at some airports (e.g. CHAN et al., 2006), will likely be relevant for a smooth and safe operation. Coplanar Doppler lidar measurements might be the solution to that.

Acknowledgments

Supplemental data

The supplement data set (https://zenodo.org/record/3901434#.XvBpd2gzabg) contains a 24-h movie (21:00 UTC 23 July to 21:00 UTC 24 July) of the horizontal wind field in a horizontal plane above the city of Stuttgart retrieved from coplanar horizontal Doppler lidar scans. The measurements were conducted within the framework of the Urban Climate under Change [UC]^2 program.

References

ADLER, B., N. KALTHOFF, 2014: Multi-scale transport processes observed in the boundary layer over a mountainous island. – Bound.-Layer Meteor. **153**, 515–537, DOI: 10.1007/s10546-014-9957-8.

ADLER, B., N. KALTHOFF, 2016: The impact of upstream flow on the atmospheric boundary layer in a valley on a mountainous island. – Bound.-Layer Meteor. **158**, 429–452, DOI: 10.1007/s10546-015-0092-y.

ADLER, B., O. KISELEVA, N. KALTHOFF, A. WIESER, 2019: Comparison of convective boundary layer characteristics from aircraft and wind lidar observations. – J. Atmos. Oceanic Technol. **36**, 1381–1399, DOI: 10.1175/JTECH-D-18-0118.1.

ADLER, B., N. KALTHOFF, O. KISELEVA, 2020: The diurnal cycle of the horizontal wind field over complex terrain detected with coplanar Doppler lidar scans. – Zenodo, published online, DOI: 10.5281/zenodo.3901434.

ADLER, B., A. GOHM, N. KALTHOFF, N. BABIĆ, U. CORSMEIER, M. LEHNER, M.W. ROTACH, M. HAID, P. MARKMANN, E. GAST, G. TSAKNAKI, G. GEORGOUSSIS, submitted: CROSSINN – a field experiment to study the three-dimensional flow structure in the Inn Valley, Austria. – Bull. Amer. Meteor. Soc.

ALLWINE, K.J., J.H. SHINN, G.E. STREIT, K.L. CLAWSON, M. BROWN, 2002: Overview of URBAN 2000: A multi-scale field study of dispersion through an urban environment. – Bull. Amer. Meteor. Soc. **83**, 521–536, DOI: 10.1175/1520-0477(2002)083<0521:OOUAMF>2.3.CO;2.

BARLOW, J.F., 2014: Progress in observing and modelling the urban boundary layer. – Urban Climate **10**, 216–240, DOI: 10.1016/j.uclim.2014.03.011.

BINGÖL, F., J. MANN, D. FOUSSEKIS, 2009: Conically scanning lidar error in complex terrain. – Meteorol. Z. **18**, 189–195, DOI: 10.1127/0941-2948/2009/0368.

CALHOUN, R., R. HEAP, M. PRINCEVAC, R. NEWSOM, H. FERNANDO, D. LIGON, 2006: Virtual towers using coherent Doppler lidar during the Joint Urban 2003 dispersion experiment. – J. Appl. Meteor. Climatol. **45**, 1116–1126, DOI: 10.1175/JAM2391.1.

CHAN, P., C. SHUN, K. WU, 2006: Operational LIDAR-based system for automatic windshear alerting at the Hong Kong International Airport. – In: 12th Conference on Aviation, Range, and Aerospace Meteorology, 6.11, Atlanta, GA. Amer. Meteor. Soc.

CREWELL, S., U. LÖHNERT, 2007: Accuracy of boundary layer temperature profiles retrieved with multifrequency multiangle microwave radiometry. – IEEE Transactions on Geoscience and Remote Sensing **45**, 2195–2201, DOI: 10.1109/TGRS.2006.888434.

DEL ÁLAMO, J.C., J. JIMÉNEZ, 2009: Estimation of turbulent convection velocities and corrections to Taylor's approximation. – J. Fluid Mech. **640**, 5–26, DOI: 10.1017/S0022112009991029.

DUNCAN JR, J.B., B.D. HIRTH, J.L. SCHROEDER, 2019: Enhanced estimation of boundary layer advective properties to improve space-to-time conversion processes for wind energy applications. – Wind Energy **22**, 1203–1218, DOI: 10.1002/we.2350.

GOHM, A., F. HARNISCH, J. VERGEINER, F. OBLEITNER, R. SCHNITZHOFER, A. HANSEL, A. FIX, B. NEININGER, S. EMEIS, K. SCHÄFER, 2009: Air pollution transport in an Alpine valley: results from airborne and ground-based observations. – Bound.-Layer Meteor. **131**, 441–463, DOI: 10.1007/s10546-009-9371-9.

HAID, M., 2019: marenha/doppler_wind_lidar_toolbox: First release (v1.0.0). – https://zenodo.org/record/3583083 or the github repository https://github.com/marenha/doppler_wind_lidar_toolbox/tree/v1.0.0. DOI: 10.5281/zenodo.3583083.

HAID, M., A. GOHM, L. UMEK, H.C. WARD, T. MUSCHINSKI, L. LEHNER, M.W. ROTACH, 2020: Foehn-cold pool interactions in the Inn Valley during PIANO IOP2. – Quart. J. Roy. Meteor. Soc. **146**, 728, DOI: 10.1002/qj.3735.

HAN, G., G. WANG, X. ZHENG, 2019: Applicability of Taylor's hypothesis for estimating the mean streamwise length scale of large-scale structures in the near-neutral atmospheric surface layer. – Bound.-Layer Meteor. **172**, 215–237, DOI: 10.1007/s10546-019-00446-3.

HANDWERKER, J., 2002: Cell tracking with TRACE3D-a new algorithm. – Atmos. Res. **61**, 15–34, DOI: 10.1016/S0169-8095(01)00100-4.

JACKSON, P.L., G. MAYR, S. VOSPER, 2013: Dynamically-driven winds. – In: CHOW, F.K., S.F. DE WEKKER, B.J. SNYDER (Eds.): Mountain weather research and forecasting. – Springer atmospheric sciences, Springer, Dordrecht, 121–218, DOI: 10.1007/978-94-007-4098-3_3.

KALTHOFF, N., B. VOGEL, 1992: Counter-current and channelling effect under stable stratification in the area of Karlsruhe. – Theor. Appl. Climatol. **45**, 113–126, DOI: 10.1007/BF00866400.

KALTHOFF, N., H.J. BINDER, M. KOSSMANN, R. VÖGTLIN, U. CORSMEIER, F. FIEDLER, H. SCHLAGER, 1998: Temporal evolution and spatial variation of the boundary layer over complex terrain. – Atmos. Env. **32**, 1179–1194, DOI: 10.1016/S1352-2310(97)00193-3.

KALTHOFF, N., B. ADLER, A. WIESER, M. KOHLER, K. TRÄUMNER, J. HANDWERKER, U. CORSMEIER, S. KHODAYAR, D. LAMBERT, A. KOPMANN, N. KUNKA, G. DICK, M. RAMATSCHI, J. WICKERT, C. KOTTMEIER, 2013: KITcube – a mobile observation platform for convection studies deployed during HyMeX. – Meteorol. Z. **22**, 633–647, DOI: 10.1127/0941-2948/2013/0542.

KHAN, M.A., B.A. ALVI, A. SAFI, I.U. KHAN, 2018: Drones for good in smart cities: A review. – In: Proc. Int. Conf. Elect., Electron., Comput., Commun., Mech. Comput. (EECCMC), 1–6.

KISELEVA, O., B. ADLER, N. KALTHOFF, M. KOHLER, A. WIESER, N. WITTKAMP, 2019: Data set of meteorological observations (wind, temperature, humidity) collected from a microwave radiometer and lidar measurements during four intensive observations periods in 2017 and 2018 in Stuttgart, Germany, under the BMBF Programme 'Urban Climate Under Change' [UC]2). – https://publikationen.bibliothek.kit.edu/1000093534, DOI: 10.5445/IR/1000093534.

KOSSMANN, M., R. VÖGTLIN, U. CORSMEIER, B. VOGEL, F. FIEDLER, H.J. BINDER, N. KALTHOFF, F. BEYRICH, 1998: Aspects of the convective boundary layer structure over complex terrain. – Atmos. Env. **32**, 1323–1348, DOI: 10.1016/S1352-2310(97)00271-9.

LAREAU, N.P., E. CROSMAN, C.D. WHITEMAN, J.D. HOREL, S.W. HOCH, W.O. BROWN, T.W. HORST, 2013: The persistent cold-air pool study. – Bull. Amer. Meteor. Soc. **94**, 51–63, DOI: 10.1175/BAMS-D-11-00255.1.

LÖHNERT, U., S. CREWELL, 2003: Accuracy of cloud liquid water path from ground-based microwave radiometry 1. dependency on cloud model statistics. – Radio Science **38**, 8041. DOI: 10.1029/2002RS002654.

LÖHNERT, U., D. TURNER, S. CREWELL, 2009: Ground-based temperature and humidity profiling using spectral infrared and microwave observations. Part I: simulated retrieval performance in clear-sky conditions. – J. Appl. Meteor. Climatol. **48**, 1017–1032, DOI: 10.1175/2008JAMC2060.1.

MENKE, R., N. VASILJEVIĆ, J. MANN, J.K. LUNDQUIST, 2019: Characterization of flow recirculation zones at the Perdigão site using multi-lidar measurements. – Atmos. Chem. Phys. **19**, 2713–2723, DOI: 10.5194/acp-19-2713-2019.

NEWSOM, R.K., D. LIGON, R. CALHOUN, R. HEAP, E. CREGAN, M. PRINCEVAC, 2005: Retrieval of microscale wind and temperature fields from single- and dual-Doppler lidar data. – J. Appl. Meteor. **44**, 1324–1345, DOI: 10.1175/JAM2280.1.

NEWSOM, R., R. CALHOUN, D. LIGON, J. ALLWINE, 2008: Linearly organized turbulence structures observed over a suburban area by dual-Doppler lidar. – Bound.-Layer Meteor. **127**, 111–130, DOI: 10.1007/s10546-007-9243-0.

PALMA, J., A.S. LOPES, V.C. GOMES, C.V. RODRIGUES, R. MENKE, N. VASILJEVIĆ, J. MANN, 2019: Unravelling the wind flow over highly complex regions through computational modeling and two-dimensional lidar scanning. – In: Journal of Physics: Conference Series, volume 1222, 012006. IOP Publishing, DOI: 10.1088/1742-6596/1222/1/012006.

PANTILLON, F., B. ADLER, U. CORSMEIER, P. KNIPPERTZ, A. WIESER, A. HANSEN, 2020: Formation of wind gusts in an extratropical cyclone in light of Doppler lidar observations and large-eddy simulations. – Mon. Wea. Rev. **148**, 353–375, DOI: 10.1175/MWR-D-19-0241.1.

POWELL, D.C., C. ELDERKIN, 1974: An investigation of the application of Taylor's hypothesis to atmospheric boundary layer turbulence. – J. Atmos. Sci. **31**, 990–1002, DOI: 10.1175/1520-0469(1974)031<0990:AIOTAO>2.0.CO;2.

SCHERER, D., F. AMENT, S. EMEIS, U. FEHRENBACH, B. LEITL, K. SCHERBER, C. SCHNEIDER, U. VOGT, 2019a: Three-dimensional observation of atmospheric processes in cities. – Meteorol. Z. **28**, 121–138, DOI: 10.1127/metz/2019/0911.

SCHERER, D., F. ANTRETTER, S. BENDER, J. CORTEKAR, S. EMEIS, U. FEHRENBACH, G. GROSS, G. HALBIG, J. HASSE, B. MARONGA, S. RAASCH, K. SCHERBER, 2019b: Urban Climate Under Change [UC]2–a national research programme for developing a building-resolving atmospheric model for entire city regions. – Meteorol. Z. **28**, 95–104, DOI: 10.1127/metz/2019/0913.

SERAFIN, S., B. ADLER, J. CUXART, S. DE WEKKER, A. GOHM, B. GRISOGONO, N. KALTHOFF, D. KIRSHBAUM, M. ROTACH, J. SCHMIDLI, OTHERS, 2018: Exchange processes in the atmospheric boundary layer over mountainous terrain. – Atmosphere **9**, 102, DOI: 10.3390/atmos9030102.

STAWIARSKI, C., K. TRÄUMNER, C. KNIGGE, R. CALHOUN, 2013: Scopes and challenges of dual-Doppler lidar wind measurements – an error analysis. – J. Atmos. Oceanic Technol. **30**, 2044–2062, DOI: 10.1175/JTECH-D-12-00244.1.

Meteorol. Z. (Contrib. Atm. Sci.)
PrePub Article, 2020

B. Adler et al.: Structures in the horizontal wind field over complex terrain

15

STEYN, D.G., J. BOTTENHEIM, R. THOMSON, 1997: Overview of tropospheric ozone in the Lower Fraser Valley, and the Pacific'93 field study. – Atmos. Env. **31**, 2025–2035, DOI: 10.1016/S1352-2310(97)00018-6.

STEYN, D.G., S.F. DE WEKKER, M. KOSSMANN, A. MARTILLI, 2013: Boundary layers and air quality in mountainous terrain. – In: CHOW, F.K., S.F. DE WEKKER, B.J. SNYDER (Eds.): Mountain Weather Research and Forecasting, Springer, Dordrecht, 261–289, DOI: 10.1007/978-94-007-4098-3_5.

STULL, R.B., 1988: An introduction to boundary layer meteorology. – Kluwer Academic Publishers, Dordrecht, The Netherlands, 666 pp.

TOWNSEND, A., 1976: The structure of turbulent shear flow. – 2nd edn. Cambridge University Press, 438 pp.

TRÄUMNER, K., T. DAMIAN, C. STAWIARSKI, A. WIESER, 2015: Turbulent structures and coherence in the atmospheric surface layer. – Bound.-Layer Meteor. **154**, 1–25, DOI: 10.1007/s10546-014-9967-6.

VESELOVSKII, I., D. WHITEMAN, A. KOLGOTIN, E. ANDREWS, M. KORENSKII, 2009: Demonstration of aerosol property profiling by multiwavelength lidar under varying relative humidity conditions. – J. Atmos. Oceanic Technol. **26**, 1543–1557, DOI: 10.1175/2009JTECHA1254.1.

WHITEMAN, C.D., J.C. DORAN, 1993: The relationship between overlying synoptic-scale flows and winds within a valley. – J. Appl. Meteor. **32**, 1669–1682, DOI: 10.1175/1520-0450(1993)032<1669:TRBOSS>2.0.CO;2.

WHITEMAN, C.D., M. LEHNER, S.W. HOCH, B. ADLER, N. KALTHOFF, T. HAIDEN, 2018a: Katabatically driven cold air intrusions into a basin atmosphere. – J. Appl. Meteor. Climatol. **57**, 435–455, DOI: 10.1175/JAMC-D-17-0131.1.

WHITEMAN, C.D., M. LEHNER, S.W. HOCH, B. ADLER, N. KALTHOFF, R. VOGT, I. FEIGENWINTER, T. HAIDEN, M.O. HILLS, 2018b: The nocturnal evolution of atmospheric structure in a basin as a larger-scale katabatic flow is lifted over its rim. – J. Appl. Meteor. Climatol. **57**, 969–989, DOI: 10.1175/JAMC-D-17-0156.1.

WILDMANN, N., S. KIGLE, T. GERZ, 2018: Coplanar lidar measurement of a single wind energy converter wake in distinct atmospheric stability regimes at the Perdigão 2017 experiment. – In: Journal of Physics: Conf. Series, volume 1037, 052006. IOP Publishing, DOI: 10.1088/1742-6596/1037/5/052006.

WITTKAMP, N., B. ADLER, N. KALTHOFF, O. KISELEVA, submitted: Mesoscale wind patterns over the complex urban terrain around Stuttgart investigated with dual-Doppler lidar profiles. – Meteorol. Z.